

Article

Modulation of Diamond PN Junction Diode with Double-Layered n-Type Diamond by Using TCAD Simulation

Caoyuan Mu ^{1,2,†}, Genzhuang Li ^{1,2,†}, Xianyi Lv ^{1,2}, Qiliang Wang ^{1,2}, Hongdong Li ¹, Luan Li ^{1,2,*} 
and Guangtian Zou ^{1,2,*}

¹ State Key Laboratory of Superhard Materials, Jilin University, Changchun 130015, China

² Shenzhen Research Institute, Jilin University, Shenzhen 518057, China

* Correspondence: liliuan@jlu.edu.cn (L.L.); gtzou@jlu.edu.cn (G.Z.)

† These authors contributed equally to this work.

Abstract: This study proposed a novel double-layer junction termination structure for vertical diamond-based PN junction diodes (PND). The effects of the geometry and doping concentration of the junction termination structure on the PNDs' electrical properties are investigated using Silvaco TCAD software (Version 5.0.10.R). It demonstrates that the electric performances of PND with a single n-type diamond layer are sensitive to the doping concentration and electrode location of the n-type diamond. To further suppress the electric field crowding and obtain a better balance between breakdown voltage and on-resistance, a double-layer junction termination structure is introduced and evaluated, yielding significantly improved electronic performances. Those results provide some useful thoughts for the design of vertical diamond PND devices.

Keywords: diamond; PN diode; double layer junction termination structure; simulation



Citation: Mu, C.; Li, G.; Lv, X.; Wang, Q.; Li, H.; Li, L.; Zou, G. Modulation of Diamond PN Junction Diode with Double-Layered n-Type Diamond by Using TCAD Simulation. *Electronics* **2024**, *13*, 1703. <https://doi.org/10.3390/electronics13091703>

Academic Editor: Francesco Giuseppe Della Corte

Received: 13 March 2024

Revised: 23 April 2024

Accepted: 24 April 2024

Published: 28 April 2024



Copyright: © 2024 by the authors. Licensee MDPI, Basel, Switzerland. This article is an open access article distributed under the terms and conditions of the Creative Commons Attribution (CC BY) license (<https://creativecommons.org/licenses/by/4.0/>).

1. Introduction

Energy consumption worldwide has become an increasingly serious problem with the booming of industry and economy. Si-based devices are currently the most widely used power devices in electrical applications. However, further improvement in the energy efficiency of Si-based power devices through device design and manufacture is a challenge due to the theoretical limits of the material [1–3]. Wide band gap materials such as diamond, Ga₂O₃, and GaN have been used in recent years for the design and fabrication of power devices because their excellent physical properties meet the growing efficiency requirements [4–9]. Diamond possesses an ultrawideband gap, high thermal conductivity, and high electric field, high carrier mobility [10–12], making it the most suitable material for high-power, high-temperature, high-voltage, and high-frequency power electronics applications [13–15].

However, the industrialization of diamond devices still faces the following key technical issues that need to be resolved: (1) the epitaxial growth of large-size single-crystal diamond wafers; (2) the preparation of high-quality and low-defect diamond wafers; (3) high efficiency and controllable n-type and p-type doping technologies; and (4) the advanced structure of power devices. First of all, increasing the wafer size can theoretically reduce the material loss caused by the production process (such as chip cutting), thus improving the utilization ratio. At the same time, the larger wafer size improves production efficiency, reduces cost, and improves yields. The single crystal size of natural diamond or high-pressure high-temperature growth is usually less than 15 mm. Recently, 1-inch, 2-inch, and 4-inch diamond wafers have been obtained through 3D homoepitaxial growth, mosaic technique, and heteroepitaxy technique, respectively [16]. Secondly, dislocation and defect density are two key factors of power semiconductor materials, especially for the high-power vertical device because the current conduction direction parallels the dislocation. Generally, the yield of power chips shows an exponential decrease with the defect

density. Also, many kinds of methods (growth parameters modulation, dislocation filter layer, epitaxial lateral overgrowth, etc.), have been developed to enhance the crystalline quality of diamond wafers [17,18].

So far, diamond-based rectifiers, e.g., Schottky barrier diodes (SBDs) have become a hot research topic [19,20]. The vertical diamond SBD with the high breakdown electric field (5.38 MV/cm) was prepared by Wang et al. using a field plate-assisted termination structure [21]. The highest current density (>60 kA/cm² at 6 V) was also reported by Makino et al. with an SPND to balance the on-resistance (R_{on}) and the breakdown voltage (V_{bd}) [22]. Furthermore, Shikata et al. confirmed the high-temperature stability of diamond SBD at 500 °C for a long work period [23]. Previous works demonstrate that the PND can provide a lower reverse leakage current, better avalanche capability, and better surge current capability than that of the SBD [24]. Also, the PN junction is usually adopted as the termination structure for SBDs. We previously proposed a novel beveled PN junction termination structure for the vertical diamond SBD, in which the Schottky contact is also located in the (100) p-type diamond while the PND is formed on the beveled (110) plane [20]. It demonstrates that the forward turn-on voltage (V_{on}) of the device is almost unchanged compared with that of conventional SBD. However, the depletion region formed by the PN junction hinders the current conduction area and slightly increases R_{on} . Since the PN junction does not conduct and inject minority carriers under forward bias, the introduction of PN junction does not degrade the reverse recovery performance. In the reverse bias state, the depletion region of the PN junction significantly alleviates the electric field concentration phenomenon and enhances the V_{bd} . However, there are rare reports on the development of (100) diamond PN junction diodes (PNDs) and Schottky PN junction structure diodes (SPND) due to the challenge of realizing high-quality n-type doped diamonds. Generally, the n-type doped diamond with an effective dopant is still a challenge currently although there exist many promising elements such as Li and Na in group I, N and P in group V, and O and S in group VI [25–27]. Considering some key factors such as the donor activation energy, dopant solubility, doping efficiency, and reproducibility, phosphorus is regarded as the most promising dopant at present. However, the doping efficiency of phosphorus in diamond at room temperature is low (50–90% compensation rate) and the ionization energy of the donor level is relatively high (0.57 eV) [28]. In addition, the hydrogen atoms in the growth atmosphere of diamond produce a passivation effect, which inhibits the ionization of phosphorus and leads to high resistivity. Finally, the doping concentration and doping efficiency on the (001) diamond are 1–2 orders of magnitude lower compared to the (113) and (111) facets. From the perspective of a power device, non-(001)-oriented diamond substrates still face problems such as small size, growth difficulty, and poor surface flatness [29]. Therefore, it requires an extremely high doping concentration to obtain the n-type (001) diamond with small resistance. On the other hand, the deteriorated crystalline quality of diamonds with high doping concentration results in the performance degradation of PNDs. Recently, a double-layer NiO was adopted to construct Ga₂O₃ heterojunction PNDs [30]. The relatively small hole concentration in the bottom NiO layer helps to enhance the V_{bd} while the high hole concentration in the top NiO is beneficial to obtain good contact and reduce the resistance.

Taking into account the challenge of high-quality n-type doped diamond, one possible route is to construct the heterojunction. In the wide-band semiconductor material system, there are some materials that are easy to realize n-type doping (with electron concentration of 10^{17} – 10^{19} cm⁻³) such as gallium oxide, gallium nitride, and zinc oxide. Therefore, these materials can also be employed instead of n-type diamonds to form heterojunctions to realize the JTE structure [20]. However, the heterojunction encounters the interface issue experimentally. Therefore, we believe that the double-layered structure is useful for improving the electrical properties of diamond PND. The first n⁻-diamond layer with relatively low doping concentration and high thickness provides a wider depletion region to sustain the reverse bias. In addition, the n⁻-diamond layer also shows better crystalline quality, which is beneficial to improve the heterojunction interface. On the other hand, the

increase in doping concentration in the n^+ -diamond layer helps to modulate the electric field distribution and improve the contact with the electrode. However, the design and manufacture of diamond PND has been little mentioned in the past decades. In this paper, we proposed a vertical diamond PND with a double-layer n-type diamond. The Silvaco technology computer-aided design (TCAD) simulation was performed to investigate the influence of different parameters on the PND. The TCAD is usually adopted in developing new semiconductor devices and their electrical characteristics to reduce costly and time-consuming wafer testing. Based on basic physical equations such as diffusion and transport equations, the simulation approach guarantees predictive accuracy over a wide range of technologies. One of the key parameters to evaluate the performances of power devices is Baliga's figure of merit ($BFOM = V_{bd}^2/R_{on}$). The thickness, doping concentration, and relative location of the n-type diamond layer and the size of the electrode were studied to enhance the electric field distribution in PND, which is beneficial to balance the R_{on} and V_{BD} .

2. Design Models and Calibration

The schematic cross-section of the diamond PNDs with single and double junction termination extensions designed by Silvaco TCAD software is shown in Figure 1a,b. The single layer junction termination structure PND (Figure 1a, named S-PND) is composed of a heavily doped diamond region (p^+ diamond substrate, $1\ \mu\text{m}$ with the hole concentration of $1 \times 10^{19}\ \text{cm}^{-3}$ at 550 K), a lightly doped diamond drift region (p^- diamond layer, $4\ \mu\text{m}$ with the hole concentration of $1 \times 10^{16}\ \text{cm}^{-3}$ at 550 K) and a single n-type diamond layer. The anode and cathode were set at the bottom of the p^+ region and the top of the n-type region, respectively. Subsequently, we carried out the design of the PND with a double-layer n-diamond structure (Figure 1b, named D-PND). On the one hand, the double-layer structure can improve the interface quality of the PN junction. On the other hand, this structure serves as the junction termination extension (JTE), which was commonly introduced for the power diode. We use the Shockley–Read–Hall Recombination, Auger Recombination, Bandgap Narrowing, Low-Field Mobility, and Parallel Electric Field Dependence model for simulation [31]. The Shockley–Read–Hall (SRH) Recombination primarily describes phonon transitions that occur in the presence of a trap (or defect) within the forbidden gap of the semiconductor. This is essentially a two-step process, the theory of which was first derived by and then by Hall. The SRH is modeled as follows:

$$R_{SRH} = \frac{pn - n_{ie}^2}{\tau_p \left[n + n_{ie} \exp\left(\frac{E_{trap}}{kT}\right) \right] + \tau_n \left[p + n_{ie} \exp\left(\frac{-E_{trap}}{kT}\right) \right]}$$

where n and p are the concentrations of electron and hole, respectively, n_{ie} is the intrinsic carrier concentration, E_{trap} is the difference between the trap energy level and the intrinsic Fermi level (default value), T is the lattice temperature in degrees Kelvin, and τ_p (2×10^{-9} in this work) and τ_n (2×10^{-9} in this work) are the electron and hole lifetimes, respectively.

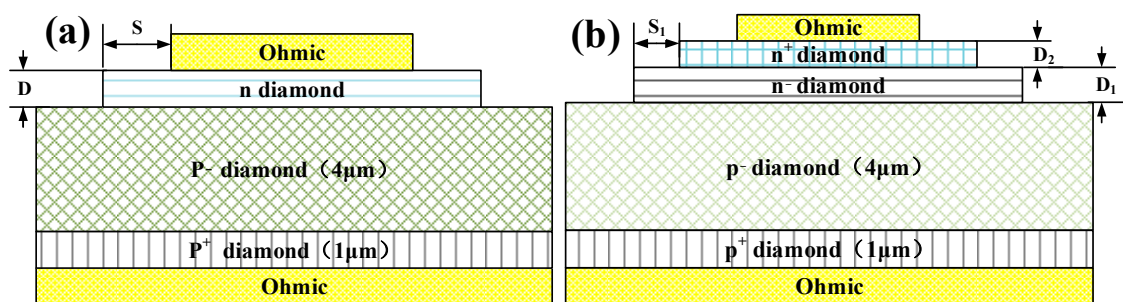


Figure 1. The schematic cross-section of the PND with single-layer n-diamond structure (S-PND) (a) and the PND with double-layered n-diamond structure (D-PND) (b).

Auger recombination occurs through a three-particle transition whereby a mobile carrier is either captured or emitted. Auger Recombination is commonly modeled using the expression:

$$R_{Auger} = \gamma_e (pn^2 - nn_{ie}^2) + \gamma_h (np^2 - pn_{ie}^2)$$

where γ_e and γ_p are the Auger coefficients of electrons (default values) and holes (default values), respectively.

The low-field mobility model is adopted according to:

$$\mu_{n0} = \mu_n \left(\frac{T}{300} \right)^{-\theta_n}$$

$$\mu_{p0} = \mu_p \left(\frac{T}{300} \right)^{-\theta_p}$$

where T is the lattice temperature, μ_n (500 and 20 for p-type and n-type diamond in this work) and μ_p (200 and 1000 for p-type and n-type diamond in this work) are the mobility of electrons and holes at 300 K. θ_n (1.5 in this work) and θ_p (1.5 in this work) are the mobility of electrons and holes at 300 K.

Firstly, the S-PND was used to evaluate the effects of electrode size and n-type diamond doping concentration and depths. For the D-PND, the dimensions and doping concentration of the double-layer n-type diamond were used for the study. The device performance (in particular, forward conduction characteristics and reverse breakdown voltage) was simulated by using the models reported in our previous work [32]. The key material parameters of the diamond were set according to reference [33]. Generally, the incomplete ionization model is adopted to evaluate the temperature dependency of dopant ionization due to the large activation energy. When the temperature increases from 250 K to 650 K, the activation of dopants will be enhanced obviously to realize a small resistance. As discussed in our previous work [34], we think that 550 K is the suitable temperature used for simulation. It is worth noting that the critical electric field for a diamond is set to be 6 MV/cm, this is attributed to the fact that the impact ionization coefficient of a diamond is not yet fully understood.

3. Results and Discussions

3.1. Modulation of the Structure Parameters for the S-PND

Firstly, the effect of the cathode size (reflected as the distance between the cathode edge and the n-type diamond edge, $S = 0, 1, 2, 3 \mu\text{m}$ in Figure 1a) on the electrical behavior of the S-PND was evaluated. For this simulation, the thickness and electron concentration of n-type diamond is set to 150 nm and $5 \times 10^{17} \text{ cm}^{-3}$ (at 550 K), respectively.

The electrical characteristics are summarized in Table 1 and shown in Figure 2. The results show that the R_{on} of the S-PNDs increases significantly from $4.51 \text{ m}\Omega \cdot \text{cm}^2$ ($S = 0 \mu\text{m}$) to $7.04 \text{ m}\Omega \cdot \text{cm}^2$ ($S = 3 \mu\text{m}$). These changes can be explained by the current density distributions at a forward bias of 8 V (Figure 3a,b). The current conduction area decreases with decreasing cathode size, which leads to an increase in R_{on} . On the other hand, the change in the size of the cathode has a positive effect on the electric field distributions of the S-PNDs. Figure 3c–f show the effect of the cathode size on the electric field distributions of S-PNDs at the reverse V_{bd} . With decreasing cathode size, new electric field peaks are generated at the cathode edge to relieve the electric field crowding around the JTE edge. It is worth noting that the electric field tends to balance between all the peaks when $S = 2 \mu\text{m}$, while it tends to concentrate around the electrode edge and leads to the degradation of the device performance when $S = 3 \mu\text{m}$. Therefore, the S-PND with $S = 2 \mu\text{m}$ can obtain the appropriate R_{on} and V_{bd} to obtain the best BFOM value.

Table 1. The simulated electric performances for the S-PNDs with different cathode sizes.

S (μm)	V_{on} (V)	R_{on} ($\text{m}\Omega\cdot\text{cm}^2$)	V_{bd} (V)	BFOM (GW/cm^2)
0	5.7	4.51	400	0.04
1	5.7	5.06	1150	0.26
2	5.7	5.86	1350	0.31
3	5.7	7.04	750	0.08

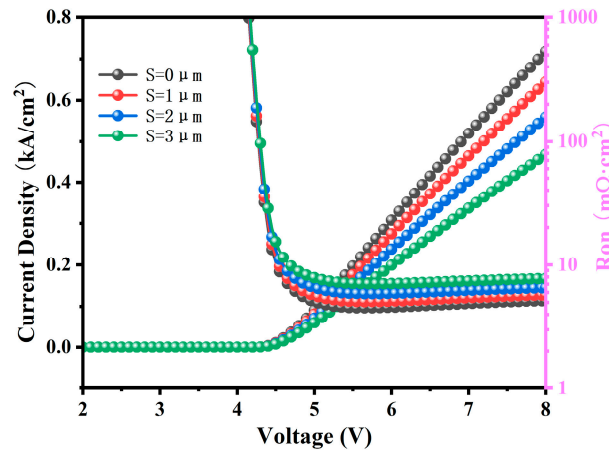


Figure 2. The I – V curves and the corresponding R_{on} for the S-PNDs with different cathode sizes.

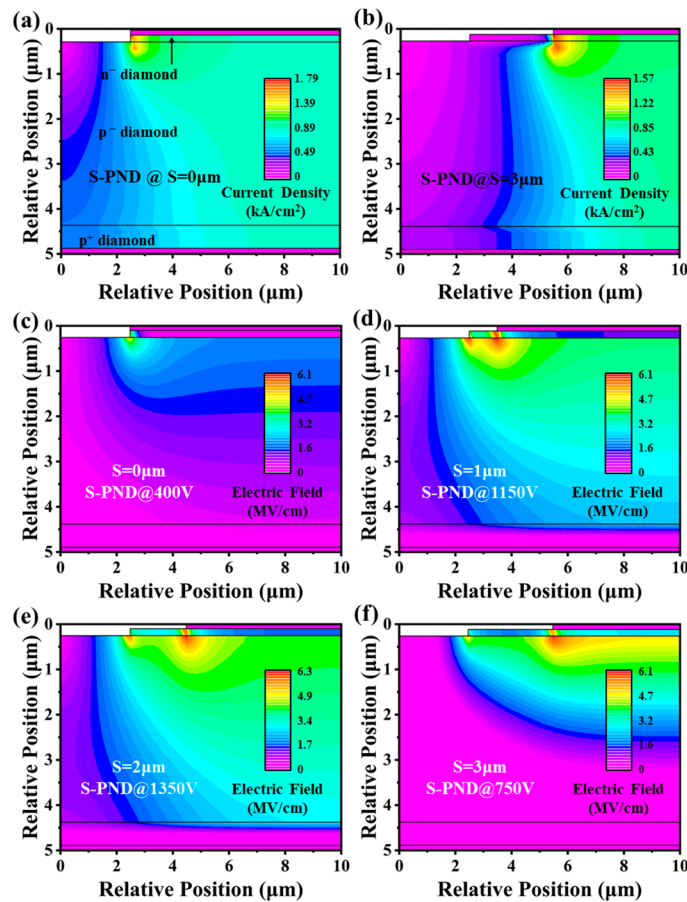


Figure 3. (a,b) are the typical current distributions under forward bias (8 V) of S-PNDs with different cathode sizes. The typical electric field distributions under V_{bd} of S-PNDs are summarized in (c–f).

In addition, considering that the device performances of S-PNDs may be influenced by the parameters of JTE, different depths ($D = 100, 150, 200$ nm) and electron concentrations ($1 \times 10^{17}, 5 \times 10^{17},$ and $1 \times 10^{18} \text{ cm}^{-3}$ at 550 K) of n-type diamond were used to perform the evaluation together. The electrical characteristics of the S-PNDs are shown in Table 2 and Figure 4. It demonstrates that the S-PND with $D = 150$ nm and electron concentration of $5 \times 10^{17} \text{ cm}^{-3}$ can simultaneously obtain a larger V_{bd} and a smaller R_{on} , resulting in the highest BFOM value. For the S-PND with a 100 nm n-type diamond layer, the n-type diamond layer is rapidly depleted and severe electric field crowding occurs at the cathode edge (Figure 4a). However, when the n-type diamond layer thickness increases to 200 nm, the controllability of the cathode electrode becomes weak, and the electric field tends to concentrate at the n-type diamond edge (Figure 4b). The uneven electric field distribution results in the rapid breakdown of S-PND. When the electron concentration of n-type diamond is relatively low ($1 \times 10^{17} \text{ cm}^{-3}$), the n-type diamond can be depleted easily. The electric field tends to accumulate at the electrode edge, causing premature breakdown of the device (Figure 4c). On the other hand, the electric field tends to concentrate at the n-type diamond layer edge when the electron concentration reaches $1 \times 10^{18} \text{ cm}^{-3}$, which also degrades the electrical performance (Figure 4d).

Table 2. The simulated electric performance for the S-PNDs with different parameters of the n-type diamond.

D (nm)	Electron Density (550 K)	R_{on} ($\text{m}\Omega \cdot \text{cm}^2$)	V_{bd} (V)	BFOM (GW/cm^2)
100	$5 \times 10^{17} \text{ cm}^{-3}$	5.32	1050	0.21
150	$1 \times 10^{17} \text{ cm}^{-3}$	8.47	500	0.03
150	$5 \times 10^{17} \text{ cm}^{-3}$	5.86	1350	0.31
150	$1 \times 10^{18} \text{ cm}^{-3}$	4.52	600	0.08
200	$5 \times 10^{17} \text{ cm}^{-3}$	6.52	900	0.13

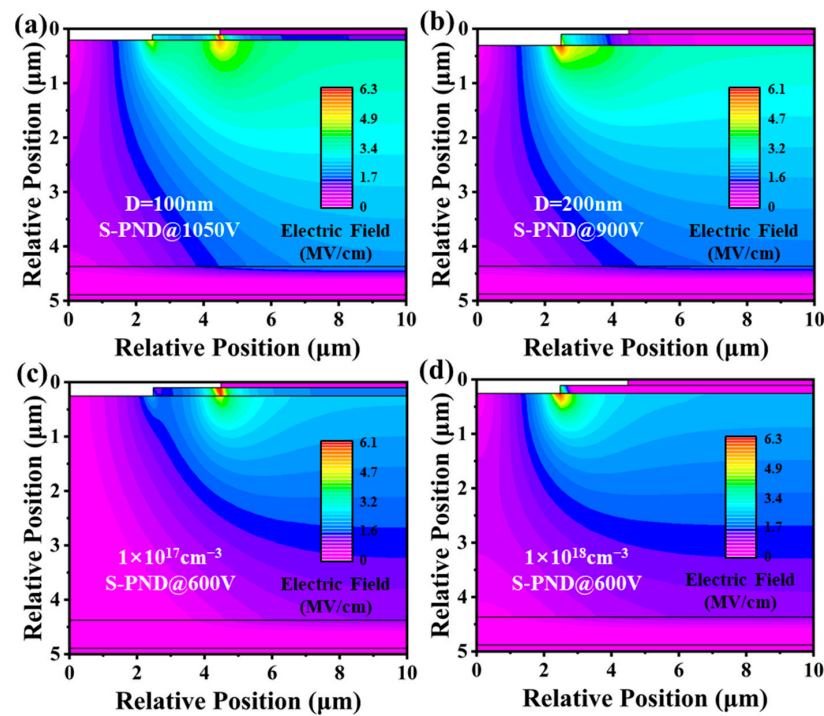


Figure 4. The typical electric field distributions under V_{bd} of S-PNDs with different parameters of the n-type diamond layer, (a) $D = 100$ nm; (b) $D = 200$ nm; electron concentration are (c) 10^{17} cm^{-3} and (d) 10^{18} cm^{-3} .

3.2. The Effects of Structure Parameters on the D-PND

Based on the above result, the performance of the PND is mainly influenced by the parameters of the n-type diamond layer. Therefore, we designed a double-layer structure PND (D-PND), consisting of n⁺-diamond layer and n⁻-diamond layer, to further improve the performances. The investigation of the performances of D-PND is carried out by first adjusting the relative distance (S_1 in Figure 1b) between the n⁺-diamond layer and the n⁻-diamond layer. The electrode length is fixed at 9 μm , and the thicknesses of the n⁻-diamond layer and n⁺-diamond layer are set to 100 nm and 50 nm, respectively. The electron concentrations of the n⁻- and n⁺-diamond layer at 550 K are chosen to be $5 \times 10^{17} \text{ cm}^{-3}$ and $1 \times 10^{18} \text{ cm}^{-3}$, respectively. The simulated results are summarized in Table 3 and shown in Figure 5. In Figure 5e, we can see that the variation in S_1 length presents no obvious effects on the forward performance of D-PND with the comparable R_{on} (Table 3), while the V_{bd} of D-PNDs is significantly influenced. These changes can be explained by the electric field distributions under V_{bd} (Figure 5). With the increase in S_1 , new electric field peaks are generated at the edges of the electrode and n⁺-diamond layer to relieve the electric field crowding in the PN contact region (Figure 5a,b). The D-PND with $S_1 = 1 \mu\text{m}$ achieves optimal performance through the balance between three electric field peaks (Figure 5c). However, the electric field peaks around the electrode edge and n⁺-diamond edge tend to merge together with further increasing S_1 , resulting in uneven electric field distribution and lower device performance (Figure 5d).

Table 3. The simulated electric performance for the D-PNDs with different S_1 .

S_1 (μm)	R_{on} ($\text{m}\Omega \cdot \text{cm}^2$)	V_{bd} (V)	BFOM (GW/cm^2)
0	5.08	400	0.03
0.5	5.08	1200	0.28
1	5.08	1450	0.42
1.5	5.08	1350	0.36

Subsequently, different doping concentrations of the double layers were used to modulate the performances of D-PNDs. The simulated electrical properties are summarized in Table 4, in which the doping concentrations of the double layers have a significant effect on the R_{on} and V_{bd} of the D-PNDs. Figure 6 provides some typical electric field distributions of the D-PNDs with different doping concentrations. Observed from Figure 6a, the n-type diamond layers are depleted totally and result in the electric field crowding around the cathode edge when the doping concentration of the n⁺-diamond layer and n⁻-diamond layer is low ($5 \times 10^{17} \text{ cm}^{-3}$ and $1 \times 10^{17} \text{ cm}^{-3}$, respectively). As the doping concentration of the n⁺-diamond layer increases to $1 \times 10^{18} \text{ cm}^{-3}$ and that of the n⁻ diamond layer increases to $5 \times 10^{17} \text{ cm}^{-3}$ (Figure 5b), the electric field distribution of the D-PND becomes uniform, leading to the highest V_{bd} and BFOM values. However, when the doping concentration of the n⁺ diamond layer was increased to $5 \times 10^{18} \text{ cm}^{-3}$ (Figure 6b), the crowding of the electric field tended to occur at the edges of the n⁺-layer and decreased the performance of the device. Therefore, the best performance of D-PND is achieved when the doping concentrations of the n⁺- and n⁻ diamond layers are $1 \times 10^{18} \text{ cm}^{-3}$ and $5 \times 10^{17} \text{ cm}^{-3}$, respectively.

Finally, the total depth of the junction termination structure was controlled to 150 nm, and the D-PNDs were modulated using different n⁺ and n⁻ diamond layer thicknesses (Table 5 and Figure 7). The results show that the electric field distributions of D-PNDs become uniform with the increasing n⁻-diamond layer thickness (D_1) when the thickness is less than 100 nm. For the D-PND with $D_1 = 50 \text{ nm}$, and $D_2 = 100 \text{ nm}$ (Figure 7a), the electric field tends to crowd at the edge of the n⁺-layer. For the D-PND with $D_1 = 75 \text{ nm}$, and $D_2 = 75 \text{ nm}$ (Figure 7b), a new electric field peak appears at the n-diamond edger, which has a positive effect on alleviating the electric field crowding. For the D-PND with $D_1 = 100 \text{ nm}$, $D_2 = 50 \text{ nm}$ (Figure 5b), the simultaneous presence of three electric field peaks at the electrode edge, the n⁺-diamond edge and the n⁻-diamond edge equalizes the electric field distribution inside the D-PND, which is conducive to obtaining excellent

V_{bd} . However, further increasing D_1 to larger than 100 nm, the electric field of the D-PNDs crowds at the edges of the PN junction contact (Figure 7c, with $D_1 = 120$ nm, $D_2 = 30$ nm) and degrade device performance.

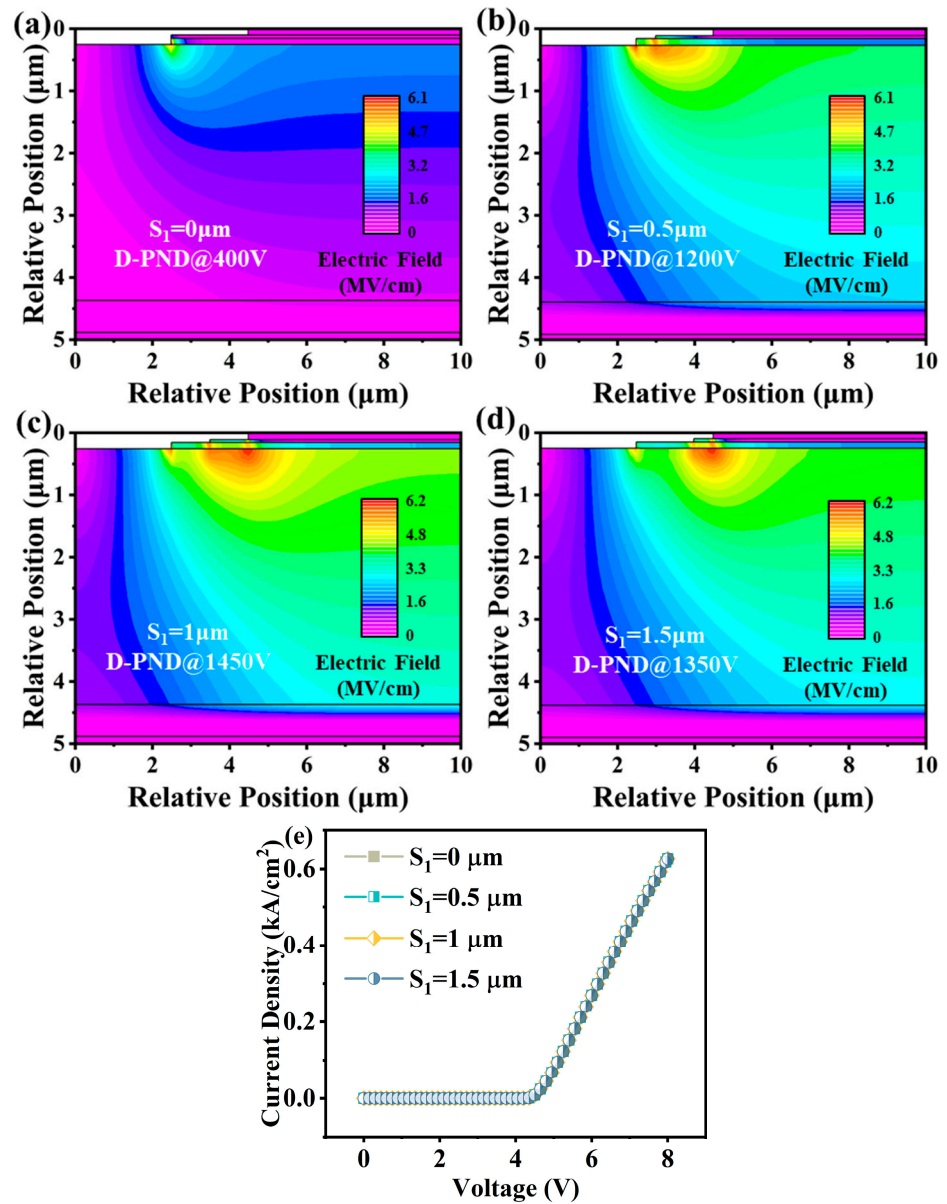


Figure 5. (a–d) The electric field distributions under V_{BD} of D-PNDs with different S_1 ; (e) the I – V curves of D-PNDs with different S_1 lengths.

Table 4. The simulated electric performances for the D-PNDs with different doping concentrations of n^+ - and n^- -diamond layers.

n^- Electron Density (550 K)	n^+ Electron Density (550 K)	R_{on} (mΩ·cm ²)	V_{bd} (V)	BFOM (GW/cm ²)
1×10^{17} cm ⁻³	5×10^{17} cm ⁻³	6.76	700	0.07
1×10^{17} cm ⁻³	1×10^{18} cm ⁻³	6.07	1050	0.18
1×10^{17} cm ⁻³	5×10^{18} cm ⁻³	4.51	400	0.02
5×10^{17} cm ⁻³	1×10^{18} cm ⁻³	5.08	1450	0.42
5×10^{17} cm ⁻³	5×10^{18} cm ⁻³	3.56	900	0.23
1×10^{18} cm ⁻³	5×10^{18} cm ⁻³	3.06	500	0.08

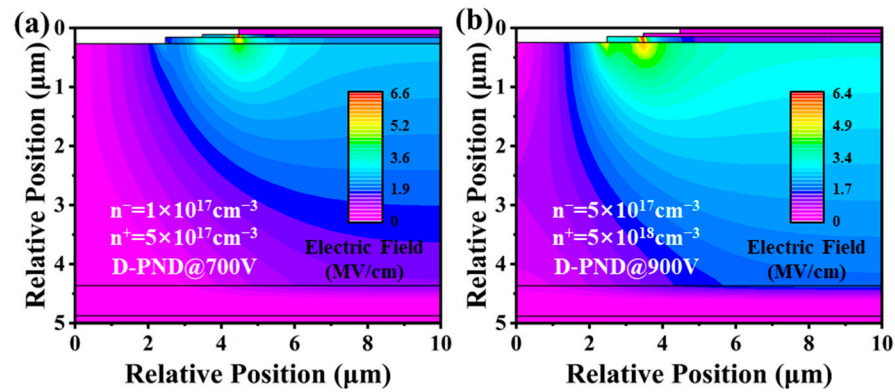


Figure 6. The electric field distributions under V_{bd} of D-PNDs with different doping concentrations of n^+ and n^- diamond layer. (a) $n^- = 10^{17} \text{ cm}^{-3}$, $n^+ = 5 \times 10^{17} \text{ cm}^{-3}$; (b) $n^- = 5 \times 10^{17} \text{ cm}^{-3}$, $n^+ = 5 \times 10^{18} \text{ cm}^{-3}$.

Table 5. The simulated electric performances for the D-PNDs with different n^+ - and n^- -diamond layer thicknesses.

D_1 (nm)	D_2 (nm)	R_{on} ($\text{m}\Omega \cdot \text{cm}^2$)	V_{bd} (V)	BFOM (GW/cm^2)
50	100	4.94	850	0.15
75	75	5.03	1150	0.26
100	50	5.08	1450	0.41
120	30	5.33	1400	0.37

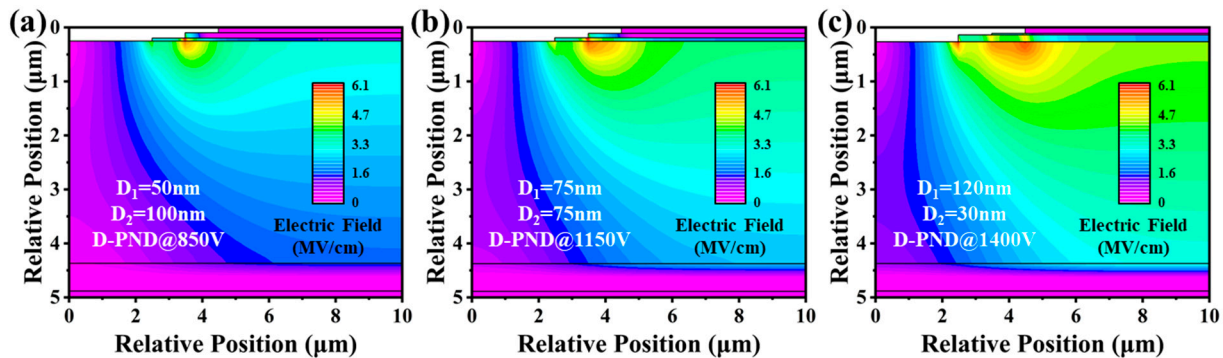


Figure 7. The electric field distributions under V_{BD} of D-PNDs with different n^+ and n^- diamond layer thicknesses. (a) $D_1 = 50 \text{ nm}$, $D_2 = 100 \text{ nm}$; (b) $D_1 = 75 \text{ nm}$, $D_2 = 75 \text{ nm}$; (c) $D_1 = 120 \text{ nm}$, $D_2 = 30 \text{ nm}$.

4. Conclusions

In summary, we report a novel diamond PND with a double-layer JTE structure and comprehensively discuss the effects of different parameters on the electrical properties of the diamond D-PND. The simulation results demonstrate that the electric performances of PND with a single n-type diamond layer are sensitive to the doping concentration and electrode location of the n-type diamond, implying the necessity of a double-layer n-type diamond. The introduction of the double JTE structure has a positive effect on regulating the R_{on} and electric field distribution of the PND, and the BFOM value is significantly increased from $0.035 \text{ GW}/\text{cm}^2$ to $0.414 \text{ GW}/\text{cm}^2$. We believe that the results are very promising to facilitate the application of diamond PNDs for high-power and high-efficiency power electronics.

Author Contributions: Conceptualization, C.M.; methodology, G.L.; formal analysis, X.L.; validation: Q.W. and H.L.; writing—original draft preparation, C.M. and G.L.; supervision, L.L.; funding acquisition, L.L. and G.Z. All authors have read and agreed to the published version of the manuscript.

Funding: This work is supported by the Natural Science Foundation of Jilin Province (No. 20240101313JC), Open Project of State Key Laboratory of Superhard Materials, Jilin University (No. 202314) and Development Program of the Ministry of Industry and Information Technology (No. 23CYJCZZ164).

Data Availability Statement: Data are contained within the article.

Acknowledgments: The authors thank T. T. Wang from Xidian University for the guidance and fruitful discussions on simulation.

Conflicts of Interest: The authors declare no conflicts of interest.

References

1. Hower, P.L.; Pendharkar, S.; Efland, T. Current status and future trends in silicon power devices. In Proceedings of the 2010 International Electron Devices Meeting, San Francisco, CA, USA, 6–8 December 2010; pp. 13.11.11–13.11.14.
2. Millán, J.; Godignon, P.; Perpiñà, X.; Pérez-Tomás, A.; Rebollo, J. A Survey of Wide Bandgap Power Semiconductor Devices. *IEEE Trans. Power Electron.* **2014**, *29*, 2155–2163. [[CrossRef](#)]
3. Zhang, Y.; Dadgar, A.; Palacios, T. Gallium nitride vertical power devices on foreign substrates: A review and outlook. *J. Phys. D Appl. Phys.* **2018**, *51*, 273001. [[CrossRef](#)]
4. Yang, H.; Ma, Y.; Dai, Y. Progress of structural and electronic properties of diamond: A mini review. *Funct. Diam.* **2022**, *1*, 150–159. [[CrossRef](#)]
5. Zhang, X.; Liao, F.; Huang, X.; Yao, D.; Du, Z.; Ma, X.; Chen, Y.; Liu, J. Design of a 6 kV Beta-Ga₂O₃ PN Heterojunction Diode with Etched Double-Layered NiO with a Figure of Merit of 10 GW cm⁻². *ECS J. Solid State Sci. Technol.* **2022**, *11*, 045012. [[CrossRef](#)]
6. Umezawa, H. Recent advances in diamond power semiconductor devices. *Mater. Sci. Semicond. Process.* **2018**, *78*, 147–156. [[CrossRef](#)]
7. Zhang, J.; Dong, P.; Dang, K.; Zhang, Y.; Yan, Q.; Xiang, H.; Su, J.; Liu, Z.; Si, M.; Gao, J.; et al. Ultra-wide bandgap semiconductor Ga₂O₃ power diodes. *Nat. Commun.* **2022**, *13*, 3900. [[CrossRef](#)] [[PubMed](#)]
8. Ma, S.; Kumaresan, Y.; Dahiya, A.S.; Lorenzelli, L.; Dahiya, R.S. Flexible Tactile Sensors Using AlN and MOSFETs Based Ultra-Thin Chips. *IEEE Sens. J.* **2023**, *23*, 23988–23994. [[CrossRef](#)]
9. Maeda, T.; Page, R.; Nomoto, K.; Toita, M.; Xing, H.G.; Jena, D. AlN quasi-vertical Schottky barrier diode on AlN bulk substrate using Al_{0.9}Ga_{0.1}N current spreading layer. *Appl. Phys. Express* **2022**, *15*, 061007. [[CrossRef](#)]
10. Amaratunga, G.A.J. A Dawn for Carbon Electronics? *Science* **2002**, *297*, 1657–1658. [[CrossRef](#)]
11. Isberg, J.; Hammersberg, J.; Johansson, E.; Wikström, T.; Twitchen, D.J.; Whitehead, A.J.; Coe, S.E.; Scarsbrook, G.A. High Carrier Mobility in Single-Crystal Plasma-Deposited Diamond. *Science* **2002**, *297*, 1670–1672. [[CrossRef](#)]
12. Inyushkin, A.V.; Taldenkov, A.N.; Ralchenko, V.G.; Bolshakov, A.P.; Koliadin, A.V.; Katrusha, A.N. Thermal conductivity of high purity synthetic single crystal diamonds. *Phys. Rev. B* **2018**, *97*, 144305. [[CrossRef](#)]
13. Shimaoka, T.; Koizumi, S.; Kaneko, J.H. Recent progress in diamond radiation detectors. *Funct. Diam.* **2022**, *1*, 205–220. [[CrossRef](#)]
14. Twitchen, D.J.; Whitehead, A.J.; Coe, S.E.; Isberg, J.; Hammersberg, J.; Wikstrom, T.; Johansson, E. High-voltage single-crystal diamond diodes. *IEEE Trans. Electron Devices* **2004**, *51*, 826–828. [[CrossRef](#)]
15. Umezawa, H.; Nagase, M.; Kato, Y.; Shikata, S.-i. High temperature application of diamond power device. *Diam. Relat. Mater.* **2012**, *24*, 201–205. [[CrossRef](#)]
16. Li, G.; Li, D.; Mu, C.; Wang, Q.; Lv, X.; Li, L.; Zou, G. Effect of step-flow modulation on the large-size single crystal diamond through mosaic growth. *Funct. Diam.* **2023**, *3*, 2279057. [[CrossRef](#)]
17. Xie, W.-L.; Lv, X.-Y.; Wang, Q.-L.; Li, L.-A.; Zou, G.-T. Relationship between spatial position of seed and growth mode in single-crystal diamond grown with an enclosed-type holder. *Chin. Phys. B* **2022**, *31*, 108106. [[CrossRef](#)]
18. Li, D.; Wang, Q.; Lv, X.; Li, L.; Zou, G. Reduction of dislocation density in single crystal diamond by Ni-assisted selective etching and CVD regrowth. *J. Alloys Compd.* **2023**, *960*, 170890. [[CrossRef](#)]
19. Makino, T.; Tanimoto, S.; Hayashi, Y.; Kato, H.; Tokuda, N.; Ogura, M.; Takeuchi, D.; Oyama, K.; Ohashi, H.; Okushi, H.; et al. Diamond Schottky-pn diode with high forward current density and fast switching operation. *Appl. Phys. Lett.* **2009**, *94*, 262101. [[CrossRef](#)]
20. Li, D.; Wang, T.; Lin, W.; Zhu, Y.; Wang, Q.; Lv, X.; Li, L.; Zou, G. Design of vertical diamond Schottky barrier diode with a novel beveled junction termination extension. *Diam. Relat. Mater.* **2022**, *128*, 109300. [[CrossRef](#)]
21. Li, Q.; Wang, J.; Shao, G.; Chen, G.; He, S.; Zhang, Q.; Zhang, S.; Wang, R.; Fan, S.; Wang, H.X. Breakdown Voltage Enhancement of Vertical Diamond Schottky Barrier Diode with Annealing Method and AlO Field Plate Structure. *IEEE Electron. Device Lett.* **2022**, *43*, 1937–1940. [[CrossRef](#)]
22. Makino, T.; Kato, H.; Tokuda, N.; Ogura, M.; Takeuchi, D.; Oyama, K.; Tanimoto, S.; Okushi, H.; Yamasaki, S. Diamond Schottky-pn diode without trade-off relationship between on-resistance and blocking voltage. *Phys. Status Solidi a* **2010**, *207*, 2105–2109. [[CrossRef](#)]
23. Ikeda, K.; Umezawa, H.; Ramanujam, K.; Shikata, S.-i. Thermally Stable Schottky Barrier Diode by Ru/Diamond. *Appl. Phys. Express* **2009**, *2*, 011202. [[CrossRef](#)]

24. Zhou, J.; He, L.; Li, X.; Pu, T.; Li, L.; Ao, J.-P. Vertical GaN Schottky barrier diodes with area-selectively deposited p-NiO guard ring termination structure. *Superlattices Microstruct.* **2021**, *151*, 106820. [[CrossRef](#)]
25. Lombardi, E.B.; Mainwood, A. A first principles study of lithium, sodium and aluminum in diamond. *Diam. Relat. Mater.* **2008**, *17*, 1349–1352. [[CrossRef](#)]
26. Hu, X.J.; Li, R.B.; Shen, H.S.; Dai, Y.B.; He, X.C. Electrical and structural properties of boron and phosphorus co-doped diamond films. *Carbon* **2004**, *42*, 1501–1506. [[CrossRef](#)]
27. Gao, N.; Gao, L.L.; Yu, H.Y. First-principles study of N and S co-doping in diamond. *Diam. Relat. Mater.* **2023**, *132*, 109651. [[CrossRef](#)]
28. Katayama-Yoshida, H.; Nishimatsu, T.; Yamamoto, T.; Orita, N. Codoping method for the fabrication of low-resistivity wide band-gap semiconductors in p-type GaN, p-type AlN and n-type diamond: Prediction versus experiment. *J. Phys. -Condens. Matter* **2001**, *13*, 8901–8914. [[CrossRef](#)]
29. Pinault-Thaury, M.-A.; Temgoua, S.; Gillet, R.; Bensalah, H.; Stenger, I.; Jomard, F.; Issaoui, R.; Barjon, J. Phosphorus-doped (113) CVD diamond: A breakthrough towards bipolar diamond devices. *Appl. Phys. Lett.* **2019**, *114*, 112106. [[CrossRef](#)]
30. Gong, H.H.; Chen, X.H.; Xu, Y.; Ren, F.-F.; Gu, S.L.; Ye, J.D. A 1.86-kV double-layered NiO/ β -Ga₂O₃ vertical p–n heterojunction diode. *Appl. Phys. Lett.* **2020**, *117*, 022104. [[CrossRef](#)]
31. Li, G.; Mu, C.; Lin, W.; Li, D.; Lv, X.; Wang, Q.; Li, L.; Zou, G. Simulation study of vertical diamond Schottky barrier diode with field plate assisted junction termination extension. *Mater. Today Commun.* **2023**, *35*, 105968. [[CrossRef](#)]
32. Wang, Q.; Wang, T.; Pu, T.; Cheng, S.; Li, X.; Li, L.; Ao, J. Hybrid-anode structure designed for a high-performance quasi-vertical GaN Schottky barrier diode. *Chin. Phys. B* **2022**, *31*, 057702. [[CrossRef](#)]
33. Miyata, K.; Nishimura, K.; Kobashi, K. Device simulation of submicrometer gate p+-i-p+ diamond transistors. *IEEE Trans. Electron Devices* **1995**, *42*, 2010–2014. [[CrossRef](#)]
34. Cai, G.; Mu, C.; Li, J.; Li, L.; Cheng, S.; Wang, Q.; Han, X. Vertical Diamond p-n Junction Diode with Step Edge Termination Structure Designed by Simulation. *Micromachines* **2023**, *14*, 1667. [[CrossRef](#)] [[PubMed](#)]

Disclaimer/Publisher’s Note: The statements, opinions and data contained in all publications are solely those of the individual author(s) and contributor(s) and not of MDPI and/or the editor(s). MDPI and/or the editor(s) disclaim responsibility for any injury to people or property resulting from any ideas, methods, instructions or products referred to in the content.